Chlorobaculum tepidum Outer Membrane Vesicles Are Likely a Significant Route for Biogenic Sulfur Transport.

Vadesse L. Noundou[1,2], Amalie Levy[2,4†], Shannon Modla[2], Yanbao Yu[5], Jing Qu[6], Thomas E. Hanson[1,2,3,*]

[1] Department of Biological Sciences, University of Delaware, Newark, DE, 19716, USA
[2] Delaware Biotechnology Institute, Newark, DE, 19713, USA
[3] School of Marine Science and Policy, University of Delaware, Newark, DE, 19716, USA
[4] Department of Chemical and Biomolecular Engineering, University of Delaware, Newark, DE, 19716, USA
[5] Department of Chemistry & Biochemistry, University of Delaware, Newark, DE, 19716, USA
[6] Advanced Materials Characterization Laboratory, University of Delaware, Newark, DE, 19716, USA

[*]Corresponding author:
Thomas E. Hanson, E-mail: tehanson@udel.edu, Tel: (302) 831-3404

†Current affiliation:
Janssen Research & Development, LLC, Malvern, PA 19355

Keywords: Chlorobiaceae, *Chlorobaculum tepidum*, sulfur globules, outer membrane vesicles, proteomics, Raman spectroscopy, NanoIR spectroscopy

ABSTRACT

Outer membrane-derived vesicles (OMVs) have been studied in different phyla of Gram-negative bacteria, most extensively in the Pseudomonadota, where they have been shown to participate in diverse biological and environmental processes. To date, the production of OMVs has not been reported in the Chlorobiaceae within the phylum Chlorobiota. *Chlorobaculum. tepidum* is the model organism for the Chlorobiaceae that synthesizes and consumes insoluble extracellular sulfur (S(0)) globules by an unknown mechanism. Here, we report evidence implicating outer membrane vesicles in biogenic S(0) globule synthesis. First we demonstrate that *Cba. tepidum* secretes OMVs in the extracellular milieu, and that OMV yield and size vary with growth conditions, particularly sulfide concentration. A core of 28 proteins involved in diverse biological processes such as cell wall biogenesis, inorganic ion transport and metabolism were found to be shared between OMVs, extracellular S(0) globules and *Cba. tepidum* intact cells. Multiple analytical methods indicated that OMVs contain S(0) and that OMVs and biogenic S(0) globules share protein and polysaccharide signatures, including lipooligosaccharides. Together these lines of evidence indicate that *Cba. tepidum*'s OMVs are one component of sulfur transport between cells and extracellular sulfur globules.

IMPORTANCE

All living cells must exchange material with their environment while maintaining cellular integrity. This is a particular challenge for materials that are not water soluble, yet many bacteria utilize insoluble materials for energy conservation and as nutrients for growth. Here we show that *Cba. tepidum* makes outer membrane vesicles and that these vesicles are likely involved in the exchange of material with extracellular elemental sulfur globules formed and consumed by *Cba. tepidum* as part of its energy metabolism based on oxidizing reduced sulfur compounds like hydrogen sulfide. These data expand our basic understanding of *Cba. tepidum*'s metabolism. As elemental sulfur is an industrial by-product with a limited number of uses, the information here may help enable the use of additional sulfur compounds by *Cba. tepidum* to drive the synthesis of biomass and/or specialty biochemicals from waste elemental sulfur by this autotrophic bacterium.

INTRODUCTION

Many microbes interact with solids as part of their energy metabolism or to obtain elements required for growth. In either case, insoluble materials must pass through the cell envelope while maintaining cellular envelope integrity. Microbe-mineral interactions often occur in the context of redox reactions for energy metabolism, e.g., the production of extracellular sulfur globules (S(0)) by sulfide oxidation and their further oxidation to sulfate by phototrophic bacteria (1) or the utilization of Fe- and Mn-oxides as terminal electron acceptors (2, 3). These microbe-mineral interactions drive many biogeochemical cycles and the bioremediation of organic and inorganic pollutants (4). In Gram-negative bacteria, outer membrane vesicles (OMVs) are one mechanism used to interact with surfaces for multiple functional outcomes (5). For example, *Acinetobacter baumannii* OMVs enriched in TonB-dependent transporters enabled the acquisition of insoluble nutrients such as iron (6). Recently, OMVs containing a truncated form of lipopolysaccharide (LPS) were implicated as a key mechanism of *Geobacter sulfurreducens*' elimination of uranium particles (7). Although OMVs have been intensively studied in heterotrophic Pseudomonadota, less is known about the production, composition, and physiological role of OMVs outside of this phylum.

Chlorobaculum tepidum (Cba. tepidum) is an anaerobic photoautotrophic Gram-negative bacterium, but little is known about the composition and metabolism of the outer membrane (OM) in this organism or the Chlorobiaceae more broadly. *Cba. tepidum* is a model organism of GSB (Green Sulfur Bacteria) due to rapid growth in culture (8), a sequenced and annotated genome (9), and genetic tools (10–12). *Cba. tepidum* utilizes a variety of inorganic sulfur compounds as electron donors to fix CO_2 through the reverse TCA cycle (13, 14). *Cba. tepidum* both forms and consumes extracellular S(0) globules, but the details of how this occurs are unclear (1). However, the enzymes catalyzing S(0) production and consumption are believed to reside in the periplasm between the OM and cell membrane (15, 16). As S(0) is extracellular, there must be a transport mechanism for S(0) to cross the outer membrane during its production

81 and consumption. Compared to many other bacteria, e.g. the Pseudomonadota, the production of
82 OMVs has not been reported in *Cba. tepidum*; their structure, chemical composition, and
83 physiological roles are unknown.
84
85 *Cba. tepidum* grows well with elemental sulfur that it has synthesized, i.e. biogenic S(0), as a
86 sole electron donor and a sub-population of cells is attached to S(0) during its utilization (1).
87 Dialysis cultivation experiments which separated *Cba. tepidum* cells from biogenic S(0) with
88 molecular weight cut-off membranes ranging from 50 to 100 kDa showed that attachment to S(0)
89 globules is required for growth or that materials larger than 100 kDa are involved in sulfur
90 shuttling between biogenic S(0) and cells (1). Time-lapse phase contrast microscopy showed that
91 while some cells directly contact biogenic S(0), individual S(0) globules can be formed and
92 consumed in cultures without direct contact by cells (17). Growth rates of cells that were not
93 attached to S(0) were the same as those attached to S(0). S(0) from *Cba. tepidum* has a proteome,
94 i.e., a collection of proteins that appear to be associated with biogenic S(0) (1). Two of these are
95 CT1320.1 and CT1305, OM proteins only found in the Chlorobiaceae and *Geobacter* spp., which
96 also rely on interactions with insoluble minerals for energy metabolism (18). A much more
97 extensive collection of S(0) associated proteins was recently catalogued (19). Spectroscopic
98 characterization of *Cba. tepidum* S(0) globules indicated the presence of proteins and
99 polysaccharides as an organic coating that was proposed to slow the conversion of amorphous
100 biogenic S(0) to crystalline sulfur (20). Together these observations indicate S(0) globule
101 formation and consumption by *Cba. tepidum* involves components that contain proteins,
102 conserved outer membrane proteins, polysaccharides, that are greater than 100 kDa in size, but
103 that are smaller than can be observed by phase-contrast microscopy. OMVs are a good candidate
104 for these components.
105
106 OMVs are small (20-300 nm) spherical structures produced by Gram-negative bacteria via OM
107 vesiculation (21). OMVs contain phospholipids, LPS or lipooligosaccharides (LOS), and outer
108 membrane proteins (OMPs). OMVs also contain cargo that may include nucleic acids (DNA and
109 RNA), periplasmic components, housekeeping proteins, and enzymes (22–24). OMVs were once
110 regarded as cell debris or microscopy artifacts. Nowadays, OMVs have been shown to
111 participate in diverse biological processes, such as transferring and delivering their components
112 to the extracellular environment (25) and host-microbe interactions (26).
113
114 Microbial production of extracellular S(0) associated with organic materials is well known, but
115 mechanistic details underlying its formation are scarce (1, 17, 20, 27–29). S(0) transport by
116 cytoplasmic membrane vesicles has been observed in Archaea, e.g. Gorlas *et al.* (30) reported
117 that *Thermococcus* species produced vesicles containing S(0) solely when S(0) was added to the
118 growth medium. They hypothesized this was to remove excess S(0) not used for growth,
119 preventing the accumulation of toxic levels in the cytoplasm. Alternatively, the formation of
120 organic associated amorphous S(0) has been proposed to be a precipitation process during sulfide

121 oxidation in the presence of organics that can occur in spent medium in the absence of cells; a
122 process called organomineralization (27, 28, 31, 32).
123
124 We hypothesize that *Cba. tepidum* produces OMVs that participate in S(0) transport between
125 cells and extracellular S(0) globules. If the hypothesis is correct, then we predict proteomic
126 analysis of OMV cargo should detect previously identified S(0) globule proteins (CT1305 and
127 CT1320.1) and that there should be substantial overlap between OMV and S(0) globule
128 proteomes. LPS or LOS should also be present in both OMVs and S(0) globules. Finally, we
129 would also expect that OMV abundance will be higher when S(0) is actively being produced or
130 consumed by *Cba. tepidum*. Here, we test these predictions through a combination of OMV
131 purification, proteomic and LPS analysis of both OMVs and S(0) globules, and OMV
132 quantification under different growth conditions. Raman spectroscopy was used to investigate
133 the chemical signatures of OMVs and S(0). The data are consistent with a model where OMVs
134 participate in S(0) globule formation. Furthermore, the results reported here provide significant
135 new information on OM structure and function outside the Pseudomonadota.
136
137 **RESULTS AND DISCUSSION**
138 ***Cba. tepidum* secretes extracellular particles during growth.**
139 While OMV secretion is considered a universal process among Gram-negative bacterial species
140 (33, 34), most observations to date are from heterotrophic members of the phylum
141 Pseudomonadota, formerly Proteobacteria (35–37). *Cba. tepidum* is a member of the phylum
142 Chlorobiota, which is sister to the phylum Bacteroidota and distantly related to the
143 Pseudomonadota. Therefore, we examined *Cba. tepidum* cultures for extracellular particles by
144 microfluidic resistive pulse sensing (MRPS) analysis of 0.2 μm culture filtrates after 8 h (lag
145 phase), 14 h (early-exponential phase), and 24 h (late-exponential phase) of growth. The number
146 of particles detected was highest during the early-exponential growth phase (14 h of growth, Fig.
147 1A) and these particles contained protein (Fig. 1B). Protein and particle concentrations displayed
148 the same pattern across growth phases and is similar to many studies indicating that OMV
149 production by different bacteria is growth phase-dependent (38–40). We chose early-exponential
150 phase samples to produce large amounts of particles for more detailed analysis because of the
151 larger population size and to minimize capturing OMVs deriving from cell death or nutrient
152 limitation during later growth stages (41–43). Direct observation of *Cba. tepidum* cells in 14 h
153 culture samples by TEM found vesicles at the outer membrane (Fig. 2A, B), consistent with
154 OMV structure in other organisms, suggesting that *Cba. tepidum* actively produces OMVs via
155 OM blebbing. Particles purified from the early-exponential imaged by negative stain TEM were
156 spherical and displayed a cavity surrounded by a stained membrane (Fig. 2C, D), further
157 evidence that particles secreted by *Cba. tepidum* are likely OMVs.

158 **Particles produced by *Cba. tepidum* are the same size as OMVs and contain**
159 **lipooligosaccharides.**

160 *Cba. tepidum* can grow on sulfide, thiosulfate, or biogenic S(0) as electron donors. Therefore, we
161 examined whether particles differed when they were purified from cultures grown on single
162 electron donors or the combination of sulfide and thiosulfate in Pf-7, the standard growth
163 condition (1, 8). *Cba. tepidum* growth rate was not significantly different between the growth
164 conditions (data not shown). Particles were characterized both by transmission electron
165 microscopy (TEM) and MRPS. TEM imaging requires sample concentration by
166 ultracentrifugation and chemical treatment prior to imaging, while MRPS provides information
167 on particle size and concentration after 0.2 µm filtration of the supernatant as the sole sample
168 preparation step. Therefore, we utilized MRPS to compare the concentration and size of OMVs
169 across growth conditions, while TEM image analysis was used to check particle morphology and
170 size. The particle size distributions by TEM (10-105 nm) and MRPS (40-125 nm) overlapped
171 (Fig. S2), with the difference likely being the size limit of detection for the MRPS cartridge
172 being ~40 nm. Particles produced when thiosulfate was the sole electron donor were slightly
173 larger by MRPS than particles released under other conditions, but the size distribution of
174 particles purified from all conditions overlapped and is consistent with published values for
175 OMVs (Fig. 3A). Regardless of the electron donor, the counted particles contained protein, with
176 a linear relationship between particle and protein concentrations (Fig. 3B), suggesting that
177 particles have a constant concentration of protein per unit of particle volume.
178
179 Lipopolysaccharide (LPS), the major component of the outer leaflet of the OM, plays a crucial
180 role in the stability and permeability of the OM and is present in OMVs. Previously, biogenic
181 S(0) produced by *Cba. tepidum* was shown to stain with an OM-specific dye (20), suggesting
182 that it contains LPS. Therefore, we tested whether particles and biogenic S(0) produced by *Cba.*
183 *tepidum* contain LPS. Tricine SDS-PAGE was used to visualize material produced by an LPS
184 purification protocol: material from *Cba. tepidum* whole cells (WC) or particles resolved in a
185 single low molecular weight band (Fig. 3C) while material purified from biogenic S(0) resolved
186 into two bands (Fig. 3D), with the lower molecular weight band migrating identically to that
187 from cells and particles. The *E. coli* purified LPS standard produced a laddered pattern
188 characteristic of an O antigen (Fig. 3C). Therefore, we conclude that *Cba. tepidum* makes
189 lipooligosaccharide (LOS), composed of lipid A and an inner core oligosaccharide (band 1).
190 *Bacteroides thetaiotamicron,* a member of the phylum Bacteroidota more closely related to *Cba.*
191 *tepidum* than *E. coli*, also synthesizes LOS (44). Similarly, Meißner *et al.* (45) showed that
192 purified OM lipid from *Chlorobium vibrioforme* had no O antigen repeating units, i.e. it is LOS.
193 The identity of band 2 observed in biogenic S(0) is unclear, but the staining method used is
194 specific for sugars, e.g. glycolipids like those in LPS and LOS. These samples did not contain
195 any material that stained with SYPRO Ruby (data not shown), indicating that the LPS
196 preparations were protein-free.
197
198 The identity of the material in the LPS preparations was further established by mass
199 spectrometry and an HPLC assay for the inner core sugar 2-ketodeoxy-octulosonic acid (KDO).

Masses consistent with lipid A were observed in electrospray ionization Fourier transform MS after mild acid hydrolysis of LOS isolated from WC, OMVs, and biogenic S(0). Different forms of lipid A were detected in each sample. The hepta-acyl form was found in WC, HS-OMV, and S(0) (*m/z* 1851, 1894, 1925, 1926, 1912), while the penta-acyl form was found only in Pf7-OMV (*m/z* 1659, 1705, 1795). The observed diversity of lipid A forms in *Cba. tepidum* suggests some differences in their acyl chain length and number depending on growth condition, which may in turn affect or be a result of OMV production (46–48). KDO was detected in all samples tested, with the highest level found in whole cells (Fig. 2E). No KDO was detected in any mock samples: PBS and chemical sulfur purchased from Sigma-Aldrich using the same reagents and buffers for preparing the samples. Taken together with the data on particle size, TEM appearance, and protein content, the detection of glycolipid staining, Lipid A, and KDO in particles produced by *Cba. tepidum* confirms that these are indeed OMVs. Detection of these signatures in biogenic S(0) supports a hypothesis where OMVs may be one route of transfer of S(0) to extracellular S(0) globules.

Proteome analysis of *Cba. tepidum* OMVs versus whole cells and biogenic Sulfur

Previously, we had shown that extracts of biogenic S(0) produced by *Cba. tepidum* contained the proteins CT1305 and CT1320.1 (1). Deeper analysis of these extracts by shotgun proteomics indicated that biogenic S(0) contained a significant proteome of at least 96 proteins (Supplemental Table S1), which is lower than the 696 S(0)-associated proteins recently identified by Lyratzakis *et al.* (19). Here, we compared new proteomic datasets for *Cba. tepidum* OMVs, biogenic S(0), and diluted whole cells of *Cba. tepidum* to control for S(0)-attached cells that are difficult to separate from biogenic S(0). The dilution factor for the WC sample was calculated based on the observed concentration of bacteriochlorophyll (Bchl) *c* in biogenic S(0), assuming that Bchl *c* in biogenic S(0) is from adherent cells. This approach enabled comparisons to identify differences and similarities between cells, OMVs, and S(0). A total of 1249 unique proteins were identified across all samples (Fig. 4A). OMVs from thiosulfate-only cultures only contained two proteins, CT0068 and CT2144, which are both outer membrane beta-barrel proteins, suggesting that electron donors might play a key role in shaping the cargo carried by OMVs. For example, Liu *et al.* (49) showed that differences in redox potential might impact the packaging of specific molecules (lipids, enzymes, proteins, toxins) into OMVs. Based on the limited proteome in thiosulfate-OMVs, this condition was excluded from further comparative analysis.

OMV proteomes from cultures grown on sulfide, sulfide + thiosulfate, purified biogenic S(0) globules, and diluted whole-cells shared 28 proteins (Table 1), which we considered to be the OMV core proteome. The functional annotations of the 28 proteins include porin activity, electron transfer activity, and trafficking of unfolded proteins. Furthermore, two periplasmic proteins, SurA (CT2264) and DegP (CT1447), identified in the initial S(0) globule proteome (Supplemental Table S1), were also found in HS-OMVs. Based on experimental evidence (50)

240 and a computational model (51), SurA is believed to be involved in the trafficking of unfolded
241 outer membrane proteins, while DegP has protease activity and is involved in the degradation of
242 misfolded proteins, preventing the accumulation of waste in the periplasm. Many of the core
243 proteins have unknown or poorly annotated functions, including CT1305, previously identified
244 in the biogenic S(0) proteome. CT1320.1 was not detected in any of the analyzed samples.
245

246 We assessed the relationship between protein composition and sample characteristics using
247 Principal Components Analysis (PCA, Fig. 4B), which incorporates label-free quantification
248 abundance data, not just presence-absence. Our analysis showed that the first two components
249 accounted for a high proportion of the total variation (87.9%) between samples. The OMV and
250 S(0) samples were well separated from whole cells on the PC1 axis (80.6% of variation). The
251 OMV and S(0) samples also separated along the PC2 axis (7.3% of variation), indicating that
252 they are distinct from one another. PSORTb v3.03 (48) was used to predict the subcellular
253 localization of proteins identified in OMVs, S(0), and whole-cell samples (Fig. 4C). Predicted
254 OM proteins are distributed to the upper left of the scatter plot indicating that they contribute to
255 sample separation along PC1 and PC2, that is these proteins drive the separation of S(0) and
256 OMV samples from whole cells. Cytoplasmic and IM proteins are predominantly distributed to
257 the center and lower right of the plot, indicating that these drive the separation of the WC
258 samples from the others (Fig. 4C). The separation between OMVs and S(0) is driven by a subset
259 of proteins from all compartments.

260 **The effect of electron donors on OMV abundance.**
261 The relationship between the proteomes of OMV and biogenic S(0) prompted us to examine
262 whether sulfide concentration modulated OMV production. We hypothesize that during growth
263 on different sulfide concentrations, *Cba. tepidum* will release more vesicles to prevent the
264 intracellular accumulation of S(0) produced by sulfide oxidation, thus playing a key role in sulfur
265 detoxification as proposed for Archaea (30). The presence of the SurA and DegP may indicate
266 that S(0) induces unfolded protein stress as another signal for OMV production. *Cba. tepidum*
267 was grown on a range of sulfide concentrations (2-7 mM), and OMVs from each sulfide
268 concentration were analyzed by MRPS. The data showed that, as sulfide concentrations are
269 increased, particle concentration increases versus 2 mM sulfide (Fig. 5A) by 2.8-fold at 4 mM
270 sulfide and ~10.7-fold at 5 mM, with no further significant increase at 7 mM. This result
271 suggests that growing *Cba. tepidum* at 5 mM sulfide produced the maximum number of particles.
272 MRPS also provides size information and documented an increase in median particle diameter
273 from 61 nm at 2 mM sulfide to 65-67 nm at 4-5 mM while those from 7 mM cultures were 88
274 nm in diameter. OMV yields can be expressed in different terms, such as lipid concentration,
275 amount of protein, total dry weight harvested, or counts by TEM, making the comparison of
276 OMV yield using all these methods simultaneously difficult because the measurements also
277 encompass non-vesicular materials (52, 53). TEM comparison of vesicles from 4 mM and 7 mM
278 cultures independently confirmed the increase in OMV concentration and volume in the 7 mM

279 sulfide OMVs (Fig. 5 C, D). Collectively, these data confirm that OMV numbers and sizes vary
280 with increased sulfide concentrations.
281
282 **Molecular Composition of Individual S(0) globules and OMVs.**
283 Conventional analysis techniques examine bulk populations of S(0) globules and OMVs instead
284 of individual particle composition. Here, the molecular composition of single S(0) globules or
285 OMVs was probed with atomic force microscopy coupled with Raman and infrared (IR)
286 spectroscopy. Raman spectroscopy is a non-destructive method that gives a linear correlation of
287 compound concentration to signal strength (31). Raman spectroscopic analysis of biogenic S(0)
288 and HS-OMVs revealed signals at 425-550 cm^{-1} (S-S, Sulfur), 580-680 cm^{-1} (C=S,
289 thiocarbonyl), 1050-1130 cm^{-1} (carbohydrate), 1220-1290 cm^{-1} (amide III), and 1660-1680 cm^{-1}
290 (amide I) (Fig. 6A). Different intensities of characteristic spectral regions showed that Sulfur,
291 polysaccharides, and protein concentration were higher in S(0) globules than in HS-OMVs. S(0)
292 may be added to a growing S(0) globule by an alternative route, possibly by excreted
293 polysulfides as suggested by Marnocha *et al.* (17). Porin proteins (e.g. OmpA) detected in Cba.
294 tepidum OMVs may provide channels through which anionic polysulfide can diffuse and
295 increase S(0) concentration. Additional organic materials may also be accumulating in S(0)
296 globules by organomineralization processes (32).

297 IR spectra for S(0) and HS-OMV preparations show characteristic bands for proteins (1400-1650
298 cm^{-1}), polysaccharides (1150-1200 cm^{-1}), and sulfoxide (1030-1060 cm^{-1}) (Fig. 6b). Sulfur is an
299 essential component of proteins; thus, sulfoxide found in these samples could originate from
300 sulfur-containing amino acids such as methionine, cysteine, and homocysteine. However, Steudel
301 *et al.* (54) collated multiple lines of evidence to indicate that bacterial S(0) globules contain long-
302 chain polythionates, which may also be the source of this signature. The bands around 1650 and
303 1460 cm^{-1} correspond to amide I and II vibrations of the peptide backbone, respectively. The
304 presence of polysaccharides and proteins is confirmed by the presence of the aliphatic group
305 C=O bonds (around 1660 cm^{-1}) (55), the weak peak around 1330-1430 cm^{-1} characteristic for a
306 hydroxyl group, and a weak C-H peak at 1370-1390 cm^{-1}. The pyranose band was observed in
307 the regions around 1150 and 1192 cm^{-1}. Though there are advantages to the usage of AFM-IR for
308 single S(0) and OMVs characterization, smaller vesicles or S(0) (15-50 nm) may not provide a
309 strong IR signal for a consistent characterization.

310 **OMVs from high sulfide cultures contain S(0).**
311 While Raman and IR spectroscopy analysis identified the presence of elemental sulfur in HS-
312 OMVs, the most basic question is whether purified OMVs indeed contain elemental sulfur in
313 significant amounts. Thus, HPLC of hexane extracts was used to quantify sulfur found in HS-
314 OMVs. HPLC analysis confirmed the presence of elemental sulfur in HS-OMV (Fig. 6C) that
315 were concentrated 20-fold from cultures. S(0) in the HS-OMV fraction was 94 $\pm$ 6 μM after
316 accounting for the centrifugal concentration of the OMV sample before extraction.
317

318 We calculated the maximum possible [S(0)] in the OMV fraction of a *Cba. tepidum* culture with
319 7 mM sulfide as follows. The particle concentration of purified OMVs at the time of sampling
320 (14 hrs) was 1.29 x 10^{12} particles/mL and the mean OMV diameter was 88 nm. The volume per
321 OMV, assuming they are spherical, is 3.82 x 10^{-16} mL. The total OMV volume per mL of culture
322 is then 4.92 x 10^{-4} mL. Different density values have been reported for biogenic S(0), 1.22 g cm^{-3}
323 (56), 1.31 g cm^{-3} (57) or 2.08 g cm^{-3} (58). Based on these values, the predicted [S(0)] if OMVs
324 were composed of solely of biogenic S(0) ranged from 18.8-32.0 mM, which is far more sulfide
325 than was provided to the culture. The observed S(0) concentration in OMVs is ~1-2% of the 7
326 mM sulfide provided to the culture, which is consistent with the hypothesis that OMVs are a
327 transient pool of S(0) with the presence of a complex proteome and LPS in these samples
328 confirming that S(0) is not the only cargo.
329
330 **Conclusions**
331 The data above clearly indicate that *Cba. tepidum*, and by extension the Chlorobiaceae,
332 synthesize LOS, secrete OMVs, and that OMVs likely contribute to material exchange between
333 cells and S(0) globules during their production and consumption. In addition, the data presented
334 here partially support our hypotheses that previously identified S(0) globule proteins would be
335 found in OMVs and that there should be substantial overlap between OMV and S(0) globule
336 proteomes. While CT1305 was found in OMVs, CT1320.1 was absent; such differences in OMV
337 protein cargo might be related to the bacterial growth stage at which OMVs were isolated or
338 difference in the proteomic sample preparation methods used. Several other pieces of evidence
339 agree with our hypotheses and indicate the roles of OMVs in sulfur metabolism: (i) OMVs and
340 S(0) globules share a substantial number of proteins; (ii) OMV abundance is higher when S(0) is
341 produced and consumed by *Cba. tepidum*; and (iii) OMVs and S(0) share a significant number of
342 chemical constituents, including elemental sulfur as documented by multiple independent
343 methods.
344
345 Taking the observations made here and by others, we propose a mechanism where *Cba. tepidum*
346 oxidizing sulfide produces OMVs to release accumulating S(0) and unfolded proteins from the
347 periplasmic space (Fig. 7). Following the accumulation of these cargos, the OM can bulge
348 outwards and pinch off as vesicles. We hypothesize that porins in the growing S(0) globules may
349 also allow for additional S(0) to be added perhaps by diffusion of polysulfides from cells through
350 porins (e.g. OmpA/CT1353 or OmpH/CT0254) detected in all OMV proteomes. Clearly,
351 additional mechanisms of transport and/or globule maturation occur, otherwise the chemical and
352 proteome compositions of OMVs and S(0) globules would be nearly identical. Previous
353 measurements of *Cba. tepidum* S(0) globule elemental composition indicate that they are > 99%
354 S (1). A maturation process may explain why purified S(0) globules contain higher relative
355 amounts of S, polysaccharides, and amides than OMVs based on the IR and Raman spectroscopy
356 data presented above. A simple possibility could be the exclusion or expulsion of water and
357 hydrophilic OMV cargos if multiple S(0) payloads condense by hydrophobic attraction.

358 Experiments to observe OMV fusion and S(0) globule maturation in over time from purified
359 OMVs and determining if S(0)-loaded OMVs can be used for growth by *Cba. tepidum* are
360 obvious next steps to further dissect this process.
361
362 **MATERIALS AND METHODS**
363 **Bacterial strain and growth conditions**
364 *Cba. tepidum* strain WT2321 was used in all cultures and grown in Pfennig's (Pf-7) medium, as
365 previously described by (59) with an anaerobic headspace composed of 5% CO_2 and 95% N_2
366 passed through a heated copper scrubber. *Cba. tepidum* cultures used for OMVs isolation were
367 incubated at 47°C with light provided by incandescent bulbs at an intensity of 20 µmol photons
368 m^{-2} s^{-1} measured with a light meter equipped with a quantum PAR sensor (LI-COR, Lincoln,
369 NE). *Cba. tepidum* liquid cultures were grown to different growth phases as noted in figure
370 legends. Electron donors (sulfide or thiosulfate) were added to individual bottles from
371 concentrated, anoxic stock solutions for biogenic S(0), sulfide and thiosulfate-only cultures.
372 Other growth conditions, such as light intensity and temperature, remained unchanged.
373
374 **Subcellular particle isolation and purification**
375 Extracellular particles were isolated and purified by differential centrifugation (53). One liter of
376 *Cba. tepidum* culture was centrifuged at 10,000 x *g* for 10 min at 4°C in a JA-14 rotor (Beckman
377 Coulter), and the supernatant was centrifuged again at 12,000 x *g* to remove cells and large
378 debris. The supernatant was filtered through a 0.22-µm pore-size polyvinylidene difluoride
379 (PVDF) filter membrane (Millipore, USA). Particles from the filtrate were concentrated by
380 ultracentrifugation at 100,000 x *g* for 2 h at 4°C using an SW32Ti rotor in an Optima LE-80K
381 centrifuge (Beckman Coulter). The pellets from different centrifuge tubes were pooled and
382 resuspended in 1 mL of 1X PBS and pelleted again by ultracentrifugation at 165,700 x *g* for 2 h
383 at 4°C in a TLA-55 rotor (Beckman Coulter). The pellet was resuspended in 500 µL of 1X PBS
384 and stored at -20°C until use. The total protein concentration of purified OMVs was determined
385 using the fluorometric Qubit protein assay (ThermoFisher Scientific) according to the
386 manufacturer's guidelines.
387
388 **Particle characterization by MRPS**
389 Particle samples for quantification from cultures were prepared by centrifugation through a 0.2
390 mm filter device at 16,000 x *g* for 2 minutes in an Eppendorf 5418 centrifuge. The flow through
391 was used diluted 100-fold with 0.02 µm filtered 1X PBS with 0.1% w/v BSA before analysis.
392 MRPS was performed using an nCS1 instrument (Spectradyne, Torrance, CA, USA) equipped
393 with disposable polydimethylsiloxane cartridges (mold ID 103S and box number 221118). The
394 running buffer was 0.2 µm filtered 1X PBS with 1% (v/v) Tween-20. Diluted OMV samples (7
395 µL) were loaded, and the particle detection threshold was set after three 10-s acquisitions. Data
396 was collected until the error associated with the concentration measurement was < 3%. The
397 collected data were analyzed with nCS1 Data Analyzer software (Spectradyne). The particle

398 distribution of the dilution buffer was also measured and subtracted from OMV sample data to
399 produce the OMV size and frequency distributions shown. Examples of raw nCS1 particle count
400 data are provided in supplemental materials (Fig. S1).
401
402 **Electron microscopic imaging of purified particles**
403 The particle suspension from *Cba. tepidum* was negatively stained with aqueous 2% (w/v) uranyl
404 acetate. Briefly, 400-mesh carbon-coated copper grids (Electron Microscopy Sciences) were
405 glow discharged using a PELCO easiGlow™ glow discharge system (Ted Pella) and then floated
406 on a drop of the vesicle suspension for several seconds. The grids were washed with four drops
407 of water and then negatively stained with aqueous 2% uranyl acetate. Samples were examined in
408 the bioimaging core facility at the University of Delaware using a Zeiss Libra 120 TEM
409 equipped with a Gatan Ultrascan1000 CCD or a Thermo Scientific Talos L120C TEM equipped
410 with a Thermo Scientific Ceta-M camera. For each analysis, at least 15 fields were imaged. To
411 examine particles attached to cells, *Cba. tepidum* culture fixed with 0.4% formaldehyde was
412 centrifuged at 10,000 x *g* for 5 minutes, the supernatant was removed, and the pellet was
413 processed for TEM imaging as described above. Particle size was determined by analysis with
414 ImageJ software.
415
416 **LPS purification and analysis**
417 LPS was extracted from a suspension of 4×10^{10} particles mL^{-1} by a previously described method
418 (60). LPS was separated by SDS-PAGE using 16% Tricine protein gels (1.0 mm, 14 wells,
419 BioRad) and Tricine SDS running buffer with LPS from *E. coli* O55:B5 as a standard
420 (InvivoGen). The gel was run at 125 V for 120 min at room temperature and stained with Pro-Q
421 Emerald 300 (Thermo Fisher) per the manufacturer's instructions. Briefly, the gel was oxidized
422 with periodic acid and then washed with 3% glacial acetic to remove residual periodate. The gel
423 was then incubated in 25-fold diluted Pro-Q Emerald 300 staining solution. Gel images were
424 collected on a BioRad ChemiDoc system using Image Lab software version 5.0. Images were
425 automatically contrast adjusted by the software and exported as a TIFF file to produce the figures
426 here.
427
428 **Mass spectrometry of lipid A**
429 Mild acid hydrolysis was used to separate lipid A from LPS/LOS by resuspending 0.6 mg of
430 lyophilized purified LPS in 1 mL sodium acetate (10 mM, pH = 4.5) and 1% w/v sodium
431 dodecyl sulfate (SDS). The suspension was boiled (100 ºC, 1h) and then lyophilized. Lyophilized
432 material was washed once with 1 mL of ice-cold acidified ethanol, followed by three washes
433 with ice-cold 95% ethanol to remove SDS from the solid material collected by centrifugation
434 (3,500 x *g*; 4 ºC; 5 min). The final lipid A samples were lyophilized before analysis by mass
435 spectrometry. Samples were reconstituted in 10 uL methanol, then diluted into 5:4:1
436 chloroform:methanol:water. Lipid A analysis was performed on an UltiMate 3000 UPLC system
437 coupled with an Orbitrap Q-Exactive (Thermo Fisher Scientific) mass spectrometer. A 5 µL

438 sample was injected by syringe at a flow rate of 0.2 mL/min, with the column temperature set at
439 40 °C. Samples were separated in isocratic mode (50:50 0.1% (v/v) formic acid in LC-MS grade
440 H_2O:0.1% (v/v) formic acid in LC-MS grade acetonitrile). After separation, the mass
441 spectrometry data were acquired on a Q-Exactive Orbitrap (Thermo Fisher Scientific) equipped
442 with heated electrospray ionization (HESI-II) operating in negative ionization mode. The HESI-
443 II was maintained at a spray voltage of -3.5 kV, and the mass range was set from 600-2200 m/z.
444 Data were processed using Thermo Scientific Xcalibur software version 3.1 (Thermo Fisher
445 Scientific). The lipid A molecular species were identified based on using observed mass to
446 charge (m/z) ratios to search the Lipid MAPS databases (61).

447 **Quantification of KDO**

448 KDO was derivatized with 1,2-diamino-4,5-methylenedioxybenzene dihydrochloride (DMB,
449 Sigma-Aldrich), and the resulting derivatives were quantified by HPLC following a previously
450 described method (62). Briefly, a KDO standard (Sigma-Aldrich), and purified LPS samples
451 were hydrolyzed using trifluoroacetic acid (TFA). DMB solution (5 mM, 125 mL) prepared
452 according to Hara et al., 1987 (63) was added to hydrolyzed samples, and the mixture was placed
453 in a heat block (50 ºC, 2.5 hrs) covered with aluminum foil. Subsequently, samples were placed
454 on ice (10 min), centrifuged (5 min, 10,000 rpm, 4 ºC), and analyzed using a Shimadzu SCL-40
455 HPLC system. A Prevail C18 (150 x 4.6 mm, 5 µm particle size, Alltech) analytical column was
456 used; 10 µL of sample was injected; separation was in isocratic mode (86% of 0.1%TFA, 7%
457 Acetonitrile, and 7% Methanol) at 1.3 mL min^{-1} for 20 min. DMB derivatives were detected by
458 fluorescence with excitation at 373 nm and emission at 448 nm.
459

460 **Raman Spectroscopy**

461 Samples (40 µL) of S(0) globules or OMVs in 1X PBS were pipetted onto aluminum foil held by
462 an HPLC screw top cap taped to a microscope slide and allowed to dry. Aluminum foil is a non-
463 reactive substrate for Raman measurements. A confocal Raman spectrometer (LabRam HR
464 Evolution, Horiba Scientific, Kyoto, Japan) was used to record data at the Surface Analysis
465 Facility, University of Delaware. A 532-nm laser was used, and the laser power applied was set
466 at 100%, which corresponds to a laser power of 20 mW on samples. Raman Spectra were
467 obtained over 5 seconds of acquisition time with a wavenumber from 400-4000 cm^{-1} with six
468 accumulations per spectrum.
469

470 **Combined Atomic Force Microscopy and Infrared Spectroscopy (AFM-IR)**

471 AFM-IR analysis was performed with a NanoIR2 instrument (Anasys Instruments, Santa
472 Barbara, CA, USA, now Bruker) at the Advanced Materials Characterization Laboratory,
473 University of Delaware. A 5 µL aliquot of samples was spread on a zinc sulfide sampling flat
474 and placed on the stage of the AFM-IR instrument. All AFM-IR measurements and images were
475 done under contact mode. A 1 µm × 1 µm scan area was imaged at a scan rate of 0.6 Hz with a
476 resolution of 384 pixels in both x and y axes. Individual AFM-IR spectra were collected using a
477 MIRcat-2400 laser (Daylight Solutions, San Diego, CA, USA) across the 900- 1900 cm-1

478 frequency range. The IR laser produced pulses of 140 ns at the repetition rate of 350 kHz.
479 Analysis Studio software (Anasys Instruments, Santa Barbara, CA, USA) was used for image
480 and spectral data collection.

481 **S(0) Globule Purification**

482 Cultures (1 L) of strain WT2321 were grown on sulfide-only Pf-7 (4 mM sulfide) in narrow-
483 mouth screw-cap bottles with an open phenolic cap and butyl rubber septa at 30 µmol photon m^{-2}
484 s^{-1} for 36 h. To qualitatively assay for the presence of sulfide, equal volumes of culture
485 supernatant were mixed with 10 mM $CuCl_2$, where the formation of a distinct grey precipitate
486 indicated the presence of sulfide greater than 0.2 mM. Sulfide was added to cultures when it was
487 no longer detectable by this assay. Cultures were transferred into sterile 250 ml centrifuge bottles
488 with o-ring sealing caps (Nalgene, Thermo Fisher Scientific). Cells and S(0) were collected by
489 centrifugation (1,000 × *g*, 10 min, 10 °C, JA-14 rotor). The supernatant was removed and cells
490 plus S(0) were suspended in a minimal volume of S-free Pf-7 that was layered over 25 ml of
491 sterile 2.5 M sucrose solution in sterile 50 ml centrifuge tubes with o-ring sealing caps (Nalgene,
492 Thermo Fisher Scientific); at a density of 1.32 g ml^{-1}, the sucrose retains cells in the supernatant
493 and selectively pellets S(0) when centrifuged (6,000 × *g,* 50 min, 4 °C, JS-13.1 rotor). The
494 supernatant was removed, and the resuspended pellet was centrifuged through 2.5 M sucrose two
495 more times. The collected S(0) pellet was washed three times to remove sucrose by suspending
496 in S-free Pf-7 and centrifuging (17,500 × *g* , 5 min, 10 °C, JS-13.1 rotor). S(0) was suspended in
497 S-free Pf-7 and immediately distributed into aliquots for characterization studies; aliquots were
498 stored at -80 °C until use.
499

500 **Proteomic profiling of OMVs, S(0) globules, and whole cells**

501 Purified OMVs, S(0) globules and whole cells pellet were dissolved in SDS buffer (2% SDS, 50
502 mM DTT, and 100 mM Tris-HCl pH 8.0) and sonicated for 3 min (pulse: 20s on, 20s off). After
503 sonication, the sample's suspension was incubated at 95 ºC for 10 min. A clear lysate was
504 obtained after centrifugation (16,000 x *g*, 10 min, 25 ºC, Eppendorf 5415 centrifuge). Proteins in
505 the lysate were processed for proteomics analysis following the E3 filter procedure described
506 recently (64). The digests were desalted using C18-based StageTips (CDS Analytical, Oxford,
507 PA). Liquid chromatography-tandem mass spectrometry (LC-MS/MS) was performed on an
508 Ultimate 3000 nanoLC system coupled to an Orbitrap Eclipse Tribrid mass spectrometer with
509 FAIMS Interface (Thermo Scientific). Peptides were separated on a C18 reversed phase column
510 (PepMap100 C18, 25 cm × 75 µm i.d., 3 µm; Thermo Scientific) at a flow rate of 250 nl/min.
511 Mobile phase A consisted of 0.1% formic acid in water. Mobile phase B consisted of 0.1%
512 formic acid in acetonitrile. A gradient separation was used: mobile phase B was held at 1% for 5
513 min, increased to 25% over 90 min, reached to 35% at 110 min, increased to 80% over 10 min,
514 then re-equilibrated at 1% mobile phase B for 15 min. For data-dependent MS acquisition, the
515 spray voltage was set to 1.8 kV, funnel RF level at 50%, and heated capillary temperature at 275
516 °C. The MS data were acquired in Orbitrap mode at 60,000 resolution, followed by MS/MS
517 acquisition of the most intense precursors for 1 s. For MS2 analysis, collision was set by HCD at

518 30% normalized collision energy (NCE). For FAIMS settings, a 3-CV experiment (-40|-55|-75)
519 was applied.

520 Peptide identification and quantitation used MaxQuant and Andromeda software (version
521 1.6.3.4) with most default settings. *Cba. tepidum* proteome database (Taxon ID 194439; 2,251
522 sequences) was obtained from UniProt Knowledgebase. The enzyme specificity was set to
523 'Trypsin'; oxidation of methionine, and acetyl (protein N-terminus) were set as variable
524 modification; carbamidomethylation of cysteine was set as fixed modification. Up to 2 missed
525 cleavages were allowed. The false discovery rate (FDR) was set to 1% for protein and peptide
526 identifications. MaxLFQ function embedded in MaxQuant was enabled for label-free
527 quantitation, and the LFQ minimum ratio count set to 1.

528 **Bioinformatic classification of identified proteins**
529 Visualization of quantitative proteomic data was mainly performed using Perseus software
530 (version 1.6.2.3) (65). The subcellular localization of each protein was predicted using the
531 PSORTb subcellular localization tool version 3.0.3 (https://www.psort.org/psortb/).
532
533 **S(0) Quantification in OMVs**
534 Three independent 20 mL cultures of *Cba. tepidum* were grown with 7 mM sulfide for 14 hrs.
535 OMVs were purified from the entire volume of each culture as above and resuspended in 20
536 microL of 1X PBS after the second ultracentrifugation. A 15 microL aliquot of OMV suspension
537 was extracted with 1 mL of hexanes (Sigma Aldrich). S(0) was quantified in the hexane phase by
538 HPLC on a 4.6 x 150 mM Prevail C18 column eluted with 90% methanol at 1 mL min^{-1}
539 following absorbance at 280 nm on a Shimadzu SCL-40 HPLC system. Sulfur powder (Sigma-
540 Aldrich) dissolved in chloroform was diluted to known concentrations in hexane to generate a
541 standard curve. The remaining OMV suspension was used for TEM imaging as described above.
542
543 **ACKNOWLEDGMENTS**
544 This research was partially supported by a National Science Foundation research grant to TEH
545 (1244373). VLN was partially supported by a grant from the W.M. Keck Foundation
546 (16A01455). ATL was supported by an NSF Graduate Research Fellowship Program award
547 (0750966). Research reported in this publication was supported by the National Institute of
548 General Medical Sciences of the National Institutes of Health under Award Numbers
549 T32GM133395 (partial support for VLN) and P20GM104316 for the Orbitrap Eclipse MS
550 instrument. Microscopy equipment was acquired with Unidel Foundation support and a Major
551 Research Instrumentation award (1828325) for the purchase of the LabRam HR Evolution.
552 Microscopy access was supported by grants from the NIH-NIGMS (P20GM103446), the
553 NIGMS (P20GM139760) and the State of Delaware. The content is solely the responsibility of
554 the authors and does not necessarily represent the official views of the W.M. Keck Foundation,
555 the National Institutes of Health, or the National Science Foundation.
556

557 **CONFLICT OF INTEREST DISCLOSURE**

558 Y.Y. is a named inventor on a patent application (PCT/US2023/020215) for the E3technology,
559 which has been licensed exclusively to CDS Analytical LLC (Oxford, PA).

560 **REFERENCES**

561 1. Hanson TE, Bonsu E, Tuerk A, Marnocha CL, Powell DH, Chan CS. 2016. Chlorobaculum
562 tepidum growth on biogenic S(0) as the sole photosynthetic electron donor. Environ
563 Microbiol 18:2856–2867.

564 2. Gralnick JA, Bond DR. 2023. Electron Transfer Beyond the Outer Membrane: Putting
565 Electrons to Rest. Annu Rev Microbiol 77:517–539.

566 3. Beblawy S, Bursac T, Paquete C, Louro R, Clarke TA, Gescher J. 2018. Extracellular
567 reduction of solid electron acceptors by Shewanella oneidensis. Mol Microbiol 109:571–
568 583.

569 4. Gadd GM. 2010. Metals, minerals and microbes: geomicrobiology and bioremediation.
570 Microbiology 156:609–643.

571 5. Schertzer JW, Whiteley M. 2013. Bacterial outer membrane vesicles in trafficking,
572 communication and the host-pathogen interaction. J Mol Microbiol Biotechnol 23:118–130.

573 6. Dhurve G, Madikonda AK, Jagannadham MV, Siddavattam D. 2022. Outer Membrane
574 Vesicles of Acinetobacter baumannii DS002 Are Selectively Enriched with TonB-
575 Dependent Transporters and Play a Key Role in Iron Acquisition. Microbiol Spectr
576 10:e0029322.

577 7. Clark MM, Paxhia MD, Young JM, Manzella MP, Reguera G. 2021. Adaptive synthesis of a
578 rough lipopolysaccharide in Geobacter sulfurreducens for metal reduction and
579 detoxification. Appl Environ Microbiol AEM0096421.

580 8. Wahlund TM, Woese CR, Castenholz RW, Madigan MT. 1991. A THERMOPHILIC
581 GREEN SULFUR BACTERIUM FROM NEW-ZEALAND HOT-SPRINGS,
582 CHLOROBIUM-TEPIDUM SP-NOV. Arch Microbiol 156:81–90.

583 9. Eisen JA, Nelson KE, Paulsen IT, Heidelberg JF, Wu M, Dodson RJ, Deboy R, Gwinn ML,
584 Nelson WC, Haft DH, Hickey EK, Peterson JD, Durkin AS, Kolonay JL, Yang F, Holt I,
585 Umayam LA, Mason T, Brenner M, Shea TP, Parksey D, Nierman WC, Feldblyum TV,
586 Hansen CL, Craven MB, Radune D, Vamathevan J, Khouri H, White O, Gruber TM,
587 Ketchum KA, Venter JC, Tettelin H, Bryant DA, Fraser CM. 2002. The complete genome
588 sequence of Chlorobium tepidum TLS, a photosynthetic, anaerobic, green-sulfur bacterium.
589 Proc Natl Acad Sci U S A 99:9509–9514.

590 10. Frigaard NU, Bryant DA. 2001. Chromosomal gene inactivation in the green sulfur
591 bacterium Chlorobium tepidum by natural transformation. Appl Environ Microbiol
592 67:2538–2544.

593 11. Hanson TE, Tabita FR. 2001. A ribulose-1,5-bisphosphate carboxylase/oxygenase
594 (RubisCO)-like protein from Chlorobium tepidum that is involved with sulfur metabolism
595 and the response to oxidative stress. Proc Natl Acad Sci U S A 98:4397–4402.

596 12. Maresca JA, Gomez Maqueo Chew A, Ponsatí MR, Frigaard N-U, Ormerod JG, Bryant DA.
597 2004. The bchU gene of Chlorobium tepidum encodes the c-20 methyltransferase in
598 bacteriochlorophyll c biosynthesis. J Bacteriol 186:2558–2566.

599 13. Evans BYMC, Buchanan BB, Arnon DI. 1966. A new ferredoxin-dependent carbon
600 reduction cycle in a photosynthetic bacterium. Proc Natl Acad Sci U S A 55:928–934.

601 14. Wahlund TM, Tabita FR. 1997. The reductive tricarboxylic acid cycle of carbon dioxide
602 assimilation: initial studies and purification of ATP-citrate lyase from the green sulfur
603 bacterium Chlorobium tepidum. J Bacteriol 179:4859–4867.

604 15. Chan L-K, Morgan-Kiss RM, Hanson TE. 2009. Functional Analysis of Three
605 Sulfide:Quinone Oxidoreductase Homologs in Chlorobaculum tepidum. J Bacteriol
606 191:1026–1034.

607 16. Shuman KE, Hanson TE. 2016. A sulfide:quinone oxidoreductase from Chlorobaculum
608 tepidum displays unusual kinetic properties. FEMS Microbiol Lett 363.

609 17. Marnocha CL, Levy AT, Powell DH, Hanson TE, Chan CS. 2016. Mechanisms of
610 extracellular S0 globule production and degradation in Chlorobaculum tepidum via dynamic
611 cell-globule interactions. Microbiology 162:1125–1134.

612 18. Reguera G, Kashefi K. 2019. The electrifying physiology of Geobacter bacteria, 30 years
613 on. Adv Microb Physiol 74:1–96.

614 19. Lyratzakis A, Meier-Credo J, Langer JD, Tsiotis G. 2023. Insights into the sulfur
615 metabolism of Chlorobaculum tepidum by label-free quantitative proteomics. Proteomics
616 e2200138.

617 20. Marnocha CL, Sabanayagam CR, Modla S, Powell DH, Henri PA, Steele AS, Hanson TE,
618 Webb SM, Chan CS. 2019. Insights Into the Mineralogy and Surface Chemistry of
619 Extracellular Biogenic S0 Globules Produced by Chlorobaculum tepidum. Front Microbiol
620 10:271.

621 21. Beveridge TJ. 1999. Structures of gram-negative cell walls and their derived membrane
622 vesicles. J Bacteriol 181:4725–4733.

623 22. Lee E-Y, Choi D-S, Kim K-P, Gho YS. 2008. Proteomics in gram-negative bacterial outer
624 membrane vesicles. Mass Spectrom Rev 27:535–555.

625 23. Veith PD, Chen Y-Y, Gorasia DG, Chen D, Glew MD, O'Brien-Simpson NM, Cecil JD,
626 Holden JA, Reynolds EC. 2014. Porphyromonas gingivalis outer membrane vesicles
627 exclusively contain outer membrane and periplasmic proteins and carry a cargo enriched
628 with virulence factors. J Proteome Res 13:2420–2432.

629 24. Balhuizen MD, Veldhuizen EJA, Haagsman HP. 2021. Outer Membrane Vesicle Induction
630 and Isolation for Vaccine Development. Front Microbiol 12:629090.

631 25. Mause SF, Weber C. 2010. Microparticles: Protagonists of a novel communication network
632 for intercellular information exchange. Circ Res 107:1047–1057.

633 26. Caruana JC, Walper SA. 2020. Bacterial membrane vesicles as mediators of microbe -
634 microbe and microbe - host community interactions. Front Microbiol 11:432.

635 27. Cron B, Henri P, Chan CS, Macalady JL, Cosmidis J. 2019. Elemental Sulfur Formation by
636 Sulfuricurvum kujiense Is Mediated by Extracellular Organic Compounds. Front Microbiol
637 10:2710.

638 28. Cosmidis J, Templeton AS. 2016. Self-assembly of biomorphic carbon/sulfur
639 microstructures in sulfidic environments. Nat Commun 7:12812.

640 29. Li W, Zhu L, Pan C, Chen W, Xu D, Kang D, Guo L, Mei Q, Zheng P, Zhang M. 2023.
641 Insights into the Superior Bioavailability of Biogenic Sulfur from the View of Its Unique
642 Properties: The Key Role of Trace Organic Substances. Environ Sci Technol
643 https://doi.org/10.1021/acs.est.2c07142.

644 30. Gorlas A, Marguet E, Gill S, Geslin C, Guigner J-M, Guyot F, Forterre P. 2015. Sulfur
645 vesicles from Thermococcales: A possible role in sulfur detoxifying mechanisms. Biochimie
646 118:356–364.

647 31. Nims C, Cron B, Wetherington M, Macalady J, Cosmidis J. 2019. Low frequency Raman
648 Spectroscopy for micron-scale and in vivo characterization of elemental sulfur in microbial
649 samples. Sci Rep 9:7971.

650 32. Cosmidis J, Nims CW, Diercks D, Templeton AS. 2019. Formation and stabilization of
651 elemental sulfur through organomineralization. Geochim Cosmochim Acta 247:59–82.

652 33. Kulp A, Kuehn MJ. 2010. Biological functions and biogenesis of secreted bacterial outer
653 membrane vesicles. Annu Rev Microbiol 64:163–184.

654 34. Yáñez-Mó M, Siljander PR-M, Andreu Z, Zavec AB, Borràs FE, Buzas EI, Buzas K, Casal
655 E, Cappello F, Carvalho J, Colás E, Cordeiro-da Silva A, Fais S, Falcon-Perez JM, Ghobrial
656 IM, Giebel B, Gimona M, Graner M, Gursel I, Gursel M, Heegaard NHH, Hendrix A,
657 Kierulf P, Kokubun K, Kosanovic M, Kralj-Iglic V, Krämer-Albers E-M, Laitinen S, Lässer
658 C, Lener T, Ligeti E, Linē A, Lipps G, Llorente A, Lötvall J, Manček-Keber M, Marcilla A,
659 Mittelbrunn M, Nazarenko I, Nolte-'t Hoen ENM, Nyman TA, O'Driscoll L, Olivan M,
660 Oliveira C, Pállinger É, Del Portillo HA, Reventós J, Rigau M, Rohde E, Sammar M,
661 Sánchez-Madrid F, Santarém N, Schallmoser K, Ostenfeld MS, Stoorvogel W, Stukelj R,
662 Van der Grein SG, Vasconcelos MH, Wauben MHM, De Wever O. 2015. Biological
663 properties of extracellular vesicles and their physiological functions. J Extracell Vesicles
664 4:27066.

665 35. Parks DH, Chuvochina M, Waite DW, Rinke C, Skarshewski A, Chaumeil P-A, Hugenholtz
666 P. 2018. A standardized bacterial taxonomy based on genome phylogeny substantially
667 revises the tree of life. Nat Biotechnol 36:996–1004.

668 36. Hug LA, Baker BJ, Anantharaman K, Brown CT, Probst AJ, Castelle CJ, Butterfield CN,
669 Hernsdorf AW, Amano Y, Ise K, Suzuki Y, Dudek N, Relman DA, Finstad KM, Amundson
670 R, Thomas BC, Banfield JF. 2016. A new view of the tree of life. Nat Microbiol 1:16048.

671 37. Oren A, Garrity GM. 2021. Valid publication of the names of forty-two phyla of
672 prokaryotes. Int J Syst Evol Microbiol 71.

673 38. McCaig WD, Koller A, Thanassi DG. 2013. Production of outer membrane vesicles and
674 outer membrane tubes by Francisella novicida. J Bacteriol 195:1120–1132.

675 39. Sharif E, Eftekhari Z, Mohit E. 2021. The effect of growth stage and isolation method on
676 properties of ClearColi^{TM} outer membrane vesicles (OMVs). Curr Microbiol 78:1602–1614.

677 40. Zavan L, Bitto NJ, Johnston EL, Greening DW, Kaparakis-Liaskos M. 2019. Helicobacter
678 pylori growth stage determines the size, protein composition, and preferential cargo
679 packaging of outer membrane vesicles. Proteomics 19:e1800209.

680 41. Siegele DA, Kolter R. 1992. Life after log. J Bacteriol 174:345–348.

681 42. Monod J. 1949. The growth of bacterial cultures. Annu Rev Microbiol 3:371–394.

682 43. Lewis K. 2000. Programmed death in bacteria. Microbiol Mol Biol Rev 64:503–514.

683 44. Jacobson AN, Choudhury BP, Fischbach MA. 2018. The Biosynthesis of
684 Lipooligosaccharide from Bacteroides thetaiotaomicron. MBio 9.

685 45. Meißner J, Fischer U, Weckesser J. 1987. The lipopolysaccharide of the green sulfur
686 bacterium Chlorobium vibrioforme f. thiosulfatophilum. Arch Microbiol 149:125–129.

687 46. Bonnington KE, Kuehn MJ. 2016. Outer membrane vesicle production facilitates LPS
688 remodeling and outer membrane maintenance in Salmonella during environmental
689 transitions. MBio 7.

690 47. Sartorio MG, Pardue EJ, Feldman MF, Haurat MF. 2021. Bacterial outer membrane
691 vesicles: From discovery to applications. Annu Rev Microbiol 75:609–630.

692 48. Elhenawy W, Bording-Jorgensen M, Valguarnera E, Haurat MF, Wine E, Feldman MF.
693 2016. LPS remodeling triggers formation of outer membrane vesicles in Salmonella. MBio
694 7.

695 49. Liu X, Jing X, Ye Y, Zhan J, Ye J, Zhou S. 2020. Bacterial vesicles mediate extracellular
696 electron transfer. Environ Sci Technol Lett 7:27–34.

697 50. Sklar JG, Wu T, Kahne D, Silhavy TJ. 2007. Defining the roles of the periplasmic
698 chaperones SurA, Skp, and DegP in Escherichia coli. Genes Dev 21:2473–2484.

699 51. Costello SM, Plummer AM, Fleming PJ, Fleming KG. 2016. Dynamic periplasmic
700 chaperone reservoir facilitates biogenesis of outer membrane proteins. Proc Natl Acad Sci U
701 S A 113:E4794–E4800.

702 52. Li M, Zhou H, Yang C, Wu Y, Zhou X, Liu H, Wang Y. 2020. Bacterial outer membrane
703 vesicles as a platform for biomedical applications: An update. J Control Release 323:253–
704 268.

705 53. Klimentová J, Stulík J. 2015. Methods of isolation and purification of outer membrane
706 vesicles from gram-negative bacteria. Microbiol Res 170:1–9.

707 54. Steudel R, Holdt G, Göbel T, Hazeu W. 1987. Chromatographic separation of higher
708 polythionates SnO62⊖(n= 3…22) and their detection in cultures ofThiobacillus
709 ferroxidans; Molecular composition of bacterial sulfur secretions. Angew Chem Int Ed Engl
710 26:151–153.

711 55. Freddi G, Tsukada M, Beretta S. 1999. Structure and physical properties of silk
712 fibroin/polyacrylamide blend films. J Appl Polym Sci 71:1563–1571.

713 56. Guerrero R, Mas J, Pedrós-Alió C. 1984. Buoyant density changes due to intracellular
714 content of sulfur in Chromatium warmingii and Chromatium vinosum. Arch Microbiol
715 137:350–356.

716 57. Mas J, van Gemerden H. 1987. Influence of sulfur accumulation and composition of sulfur
717 globule on cell volume and buoyant density of Chromatium vinosum. Arch Microbiol
718 146:362–369.

719 58. Meyer B. 1976. Elemental sulfur. Chem Rev 76:367–388.

720 59. Chan L-K, Weber TS, Morgan-Kiss RM, Hanson TE. 2008. A genomic region required for
721 phototrophic thiosulfate oxidation in the green sulfur bacterium Chlorobium tepidum (syn.
722 Chlorobaculum tepidum). Microbiology 154:818–829.

723 60. Yi EC, Hackett M. 2000. Rapid isolation method for lipopolysaccharide and lipid A from
724 gram-negative bacteria. Analyst 125:651–656.

725 61. Sud M, Fahy E, Cotter D, Brown A, Dennis EA, Glass CK, Merrill AH Jr, Murphy RC,
726 Raetz CRH, Russell DW, Subramaniam S. 2007. LMSD: LIPID MAPS structure database.
727 Nucleic Acids Res 35:D527-32.

728 62. Bucsella B, Hoffmann A, Zollinger M, Stephan F, Pattky M, Daumke R, Heiligtag FJ, Frank
729 B, Bassas-Galia M, Zinn M, Kalman F. 2020. Novel RP-HPLC based assay for selective
730 and sensitive endotoxin quantification. Anal Methods 12:4621–4634.

731 63. Hara S, Yamaguchi M, Takemori Y, Furuhata K, Ogura H, Nakamura M. 1989.
732 Determination of mono-O-acetylated N-acetylneuraminic acids in human and rat sera by
733 fluorometric high-performance liquid chromatography. Anal Biochem 179:162–166.

734 64. Martin KR, Le HT, Abdelgawad A, Yang C, Lu G, Keffer JL, Zhang X, Zhuang Z, Asare-
735 Okai PN, Chan CS, Batish M, Yu Y. 2024. Development of an efficient, effective, and
736 economical technology for proteome analysis. Cell Rep Methods 4:100796.

737 65. Tyanova S, Temu T, Sinitcyn P, Carlson A, Hein MY, Geiger T, Mann M, Cox J. 2016. The
738 Perseus computational platform for comprehensive analysis of (prote)omics data. Nat
739 Methods 13:731–740.

740

741
742 **FIGURES**

743
744
745
746
747
748
749
750
751
752
753
754

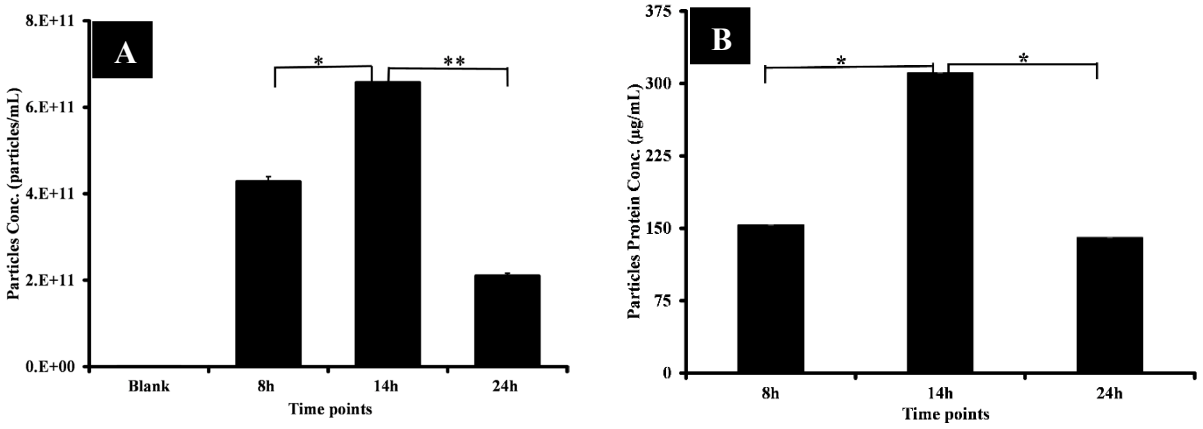

Figure 1. The effect of *Cba. tepidum* growth phase on extracellular particle concentration in cultures and protein concentration in purified particle preparations . **A.** Extracellular particles concentration from different growth phases. **B.** Total protein concentration of particles purified at different growth phases. a and b error bars represent the standard error, n=3. * and **, represent $p < 0.05$ and $p < 0.01$, respectively.

755
756

757

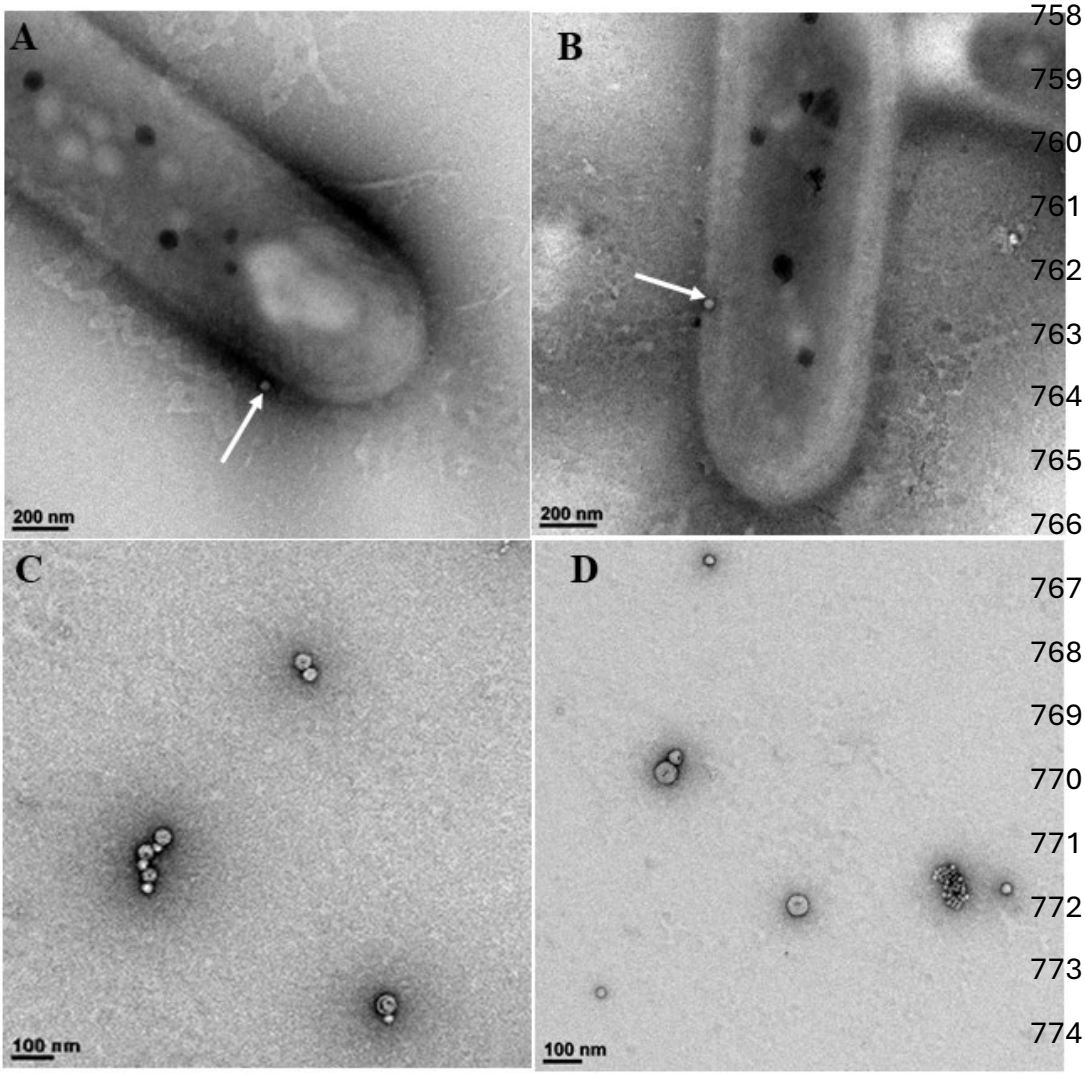

758
759
760
761
762
763
764
765
766
767
768
769
770
771
772
773
774

Figure 2. Transmission electron microscopy images of *Cba. tepidum*'s OMVs. **A.** , **B.** TEM images show spherical OMVs budding out of rod-shaped *Cba. tepidum* after 8h and 14h of growth, respectively (white arrows). **C.** , **D.** TEM analysis of OMVs purified via serial ultracentrifugation from 8h and 14h of *Cba. tepidum* culture, respectively.

775

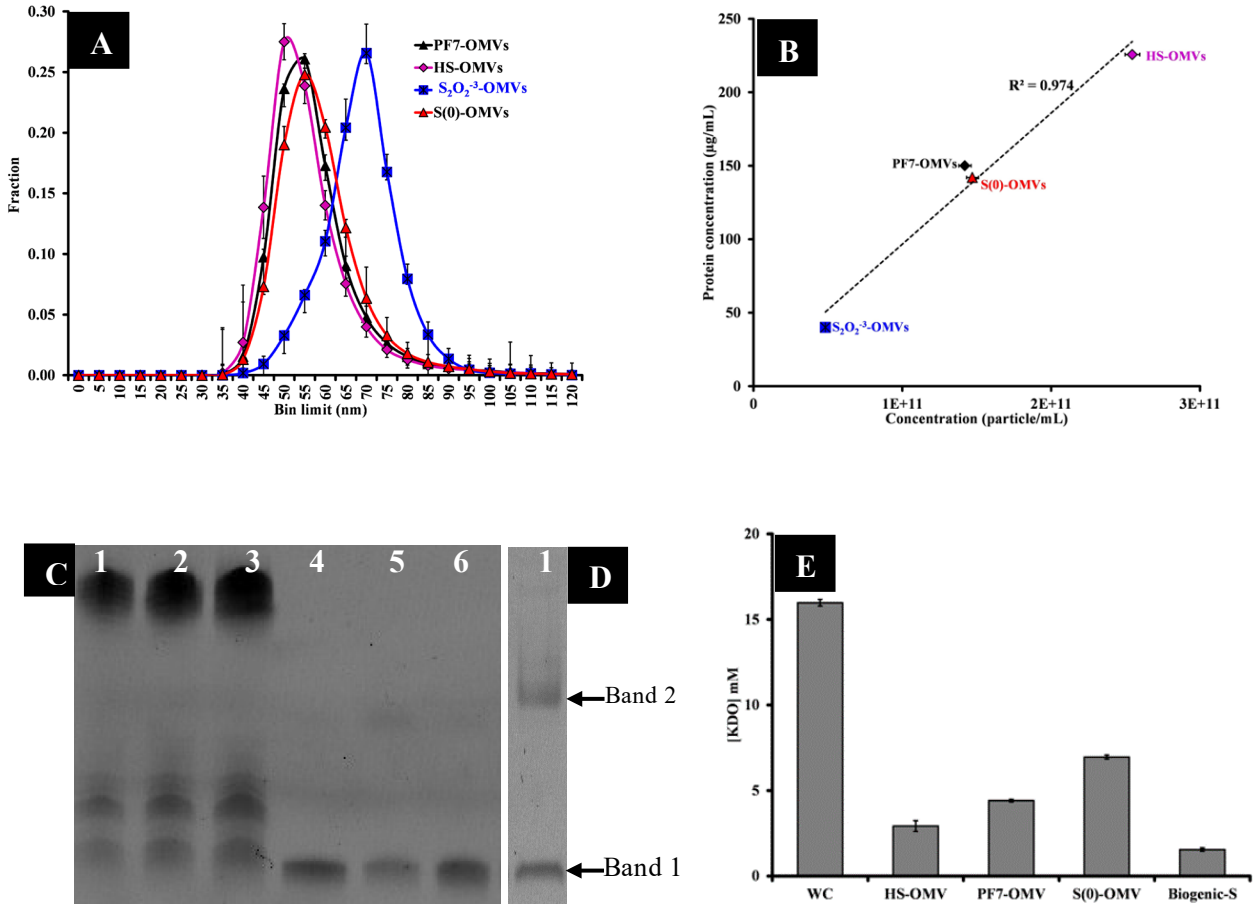

Figure 3. Physical characterization of *Cba. tepidum*'s OMVs. **A.** MRPS-based size distribution of particles purified from *Cba. tepidum* cultures grown under different electron donor. Points are the fraction of total particles found in a size class with the standard deviation from three biological replicates. **B.** Linear regression of protein concentration vs. particles concentration in suspensions purified from different growth conditions. **C. , D.** Analysis of lipopolysaccharide (LPS) profile by tricine (16%) SDS-PAGE after staining with the Pro-Q Emerald 300 LPS staining kit. Lane 1-3 are 2.5 µg, 5 µg and 10 µg respectively, of *E.coli* K-12 LPS standard. Lane 4-6 are LOS purified from HS-OMV, Pf7-OMV, whole cell respectively and biogenic sulfur (**D**). The thick band at the bottom represents the lipid A core and is intact in all samples. **E.** Quantification of KDO concentration in LPS samples. Each data point represents the measured peak area of a given KDO concentration. Bars represent standard error, n=3.

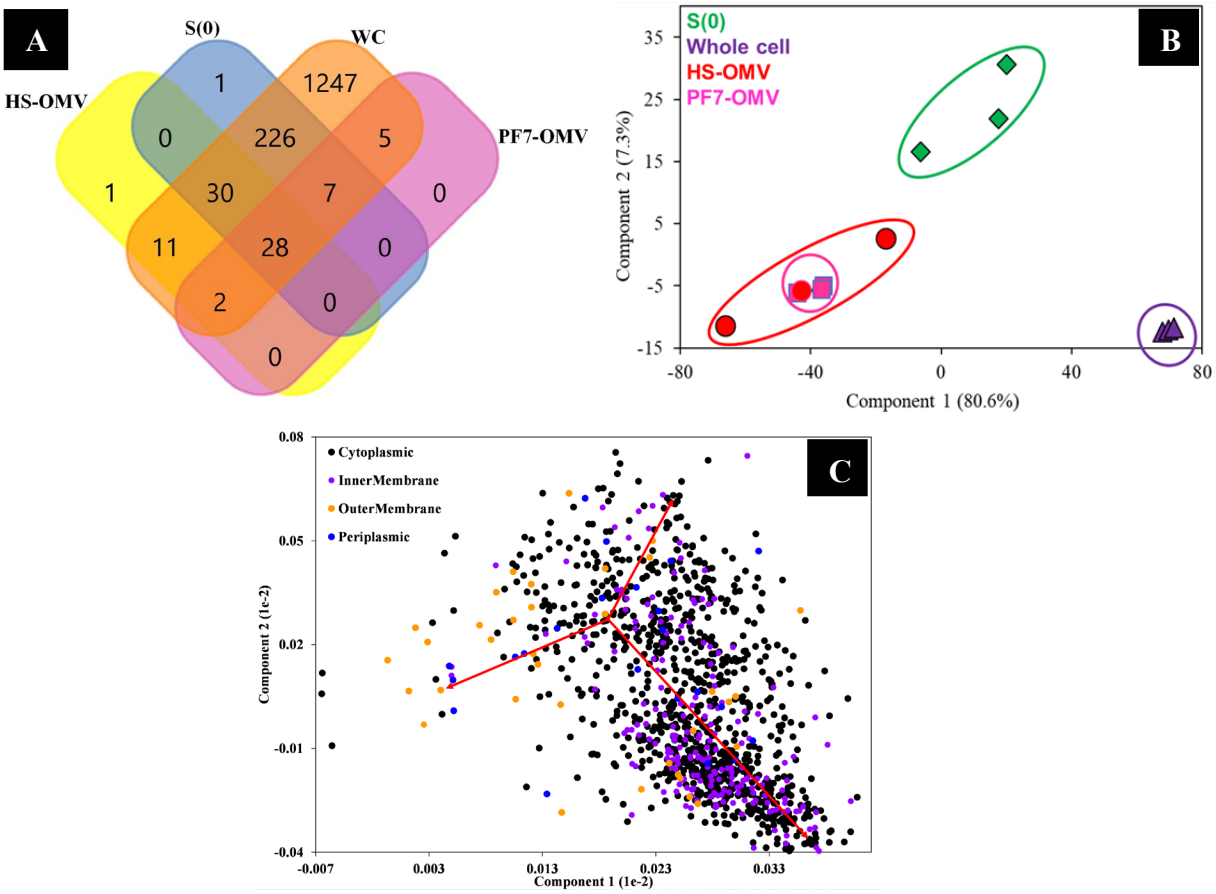

Figure 4. Comparative proteome analysis of *Cba. tepidum* whole cells, OMVs generated during growth on sulfide and on Pf-7, and biogenic sulfur. **A.** Venn diagram specifies shared and exclusive proteins found in different samples. **B.** Principal component analysis (PCA) of WC, S(0), and OMVs samples based on label free quantification of individual protein abundance. The first and the second components segregate the samples and account for 80.6% and 7.3% of the variability. **C.** Proteins driving the segregation between WC, S(0), and OMVs. Proteins are colored based on their predicted localization. For clarity, proteins with unknown localization were omitted. Arrows indicate the direction of the majority of proteins driving the difference between the 3 clusters. Arrowheads closer to a specific protein or group of proteins indicate those proteins are more abundant in those samples.

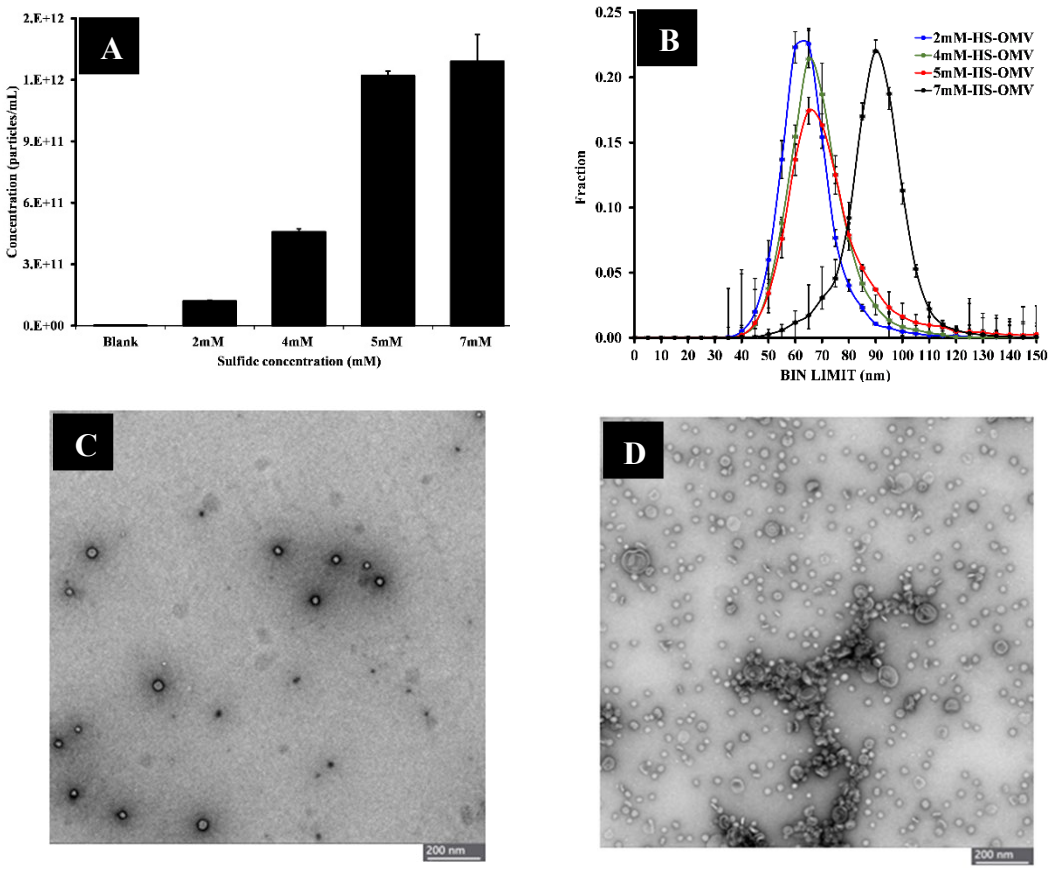

Figure 5. OMVs yield, and sizes vary with increase sulfide concentration. **A.** Dose response curve to sulfide concentration and corresponding particles concentration. **B.** MRSP-based size distribution of particles purified from *Cba. tepidum* cultures grown for 14 h under different sulfide concentration. **C.**; **D.** TEM analysis of OMVs purified via serial ultracentrifugation from 4 mM and 7 mM sulfide culture of *Cba. tepidum*, respectively.

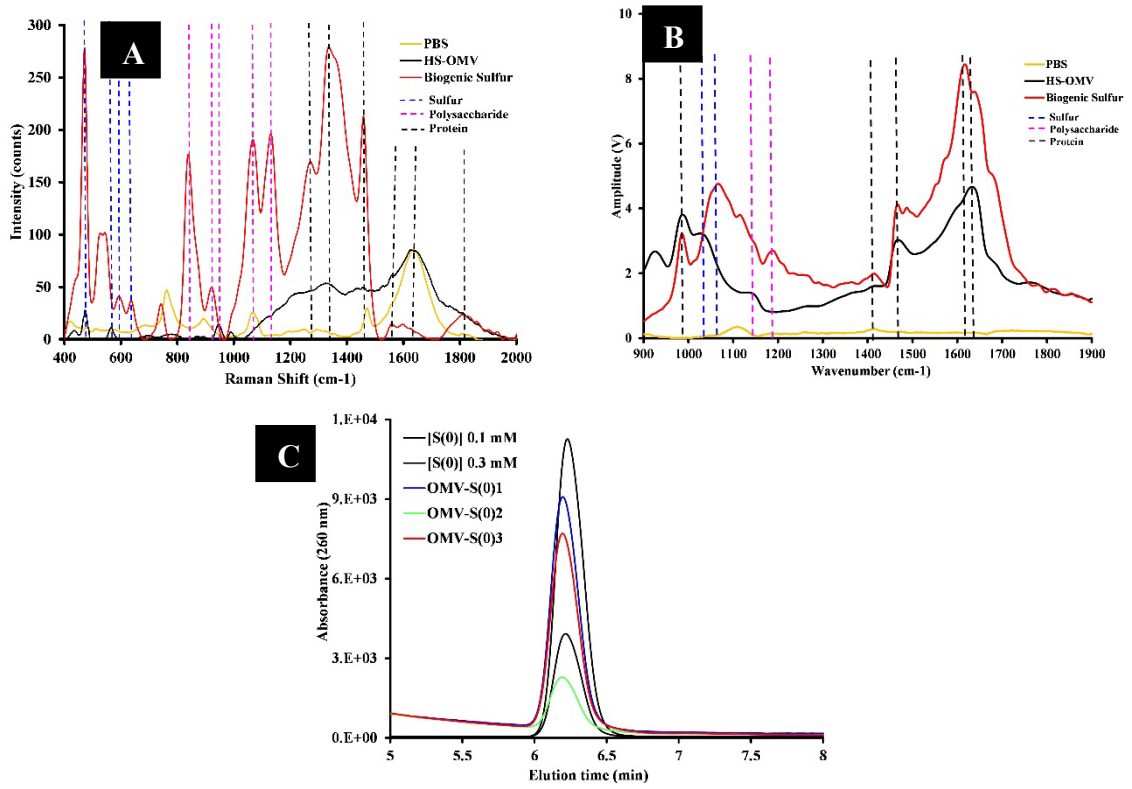

Figure 6. OMV and S(0) share significant number of chemical constituents and contain sulfur. Characteristic scattering **(A)** or absorption **(B)** peaks for purified OMVs (colored black), S(0) (colored red), and PBS (colored yellow). Absorption spectra of sulfur (blue dotted line), polysaccharide (pink dotted line) and protein (black dotted line). **(C)** Chromatograms of 0.1 and 0.3-mM elemental sulfur standards and OMVs samples. The peak at ~6.2 min increases with increasing concentration of S(0) and is assigned to elemental sulfur.

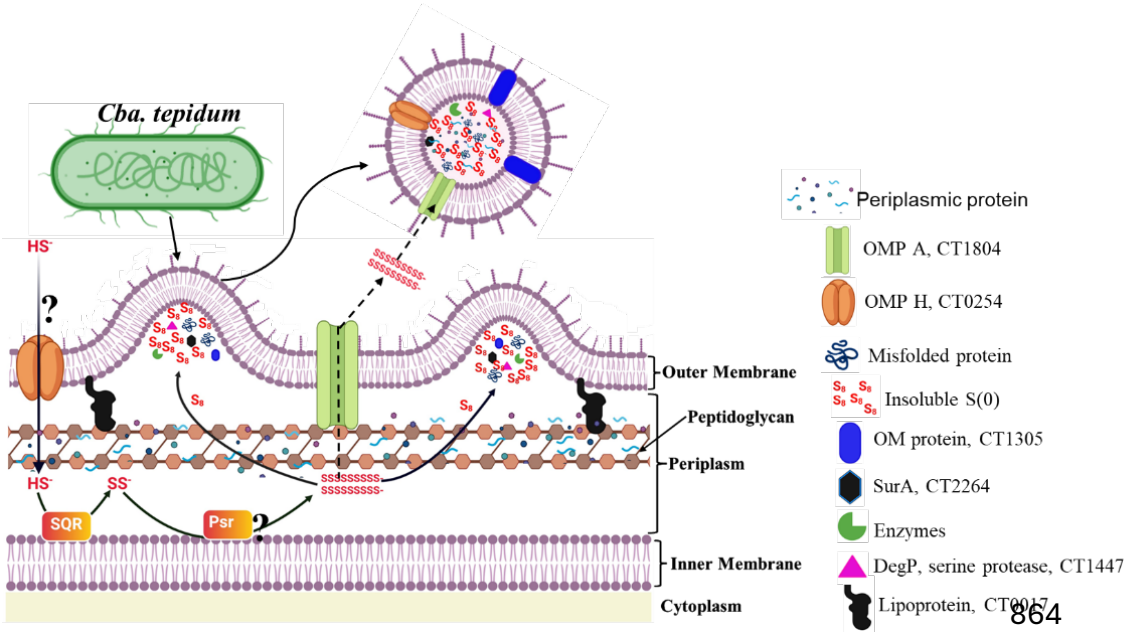

Figure 7. Summary of the proposed OMV S(0) transport mechanism. The dashed arrow shows the alternative route through which polysulfide may exit the periplasmic space and enter either OMVs or S(0) globules. SQR = sulfide:quinone oxidoreductase (CT0117 and CT1087), Psr = putative polysulfide oxidoreductase complex (CT0496-CT0494).

869

Locus Tag	Uniprot ID	PSORTb Result	Description
CT0017	Q8KGF1	Unknown	Outer membrane lipoprotein BamD-like domain-containing protein
CT0068	Q8KGA0	Unknown	Hemagglutinin-related protein
CT0073	Q8KG95	Unknown	Cytochrome c-555, membrane-bound
CT0075	Q8KG93	Periplasmic	Cytochrome c-555
CT0254	Q8KFR8	Unknown	Outer membrane protein OmpH
CT0517	Q8KF15	Outer Membrane	Tia invasion determinant-related protein
CT0529	Q8KF03	Cytoplasmic	Co-chaperonin GroES
CT0530	Q8KF02	Cytoplasmic	Chaperonin GroEL
CT0636	Q8KEQ0	Periplasmic	Protein TolB homolog
CT0638	Q8KEP8	Outer Membrane	Peptidoglycan-associated lipoprotein
CT0640	Q8KEP6	Unknown	Outer membrane lipoprotein BamD-like domain-containing protein
CT0865	Q8KE27	Cytoplasmic	Adenylylsulfate reductase, alpha subunit
CT0918	Q8KDX6	Extracellular	Pentapeptide repeat family protein
CT0935	Q8KDV9	Outer Membrane	TonB-dependent receptor-related protein
CT0984	Q8KDR1	Outer Membrane	Uncharacterized protein
CT1017	Q8KDM9	Unknown	Sulfur oxidation protein SoxY
CT1018	Q8KDM8	Unknown	Sulfur oxidation protein SoxZ
CT1054	Q8KDJ6	Inner Membrane	Carboxyl-terminal protease
CT1157	Q8KD97	Unknown	DUF4136 domain-containing protein
CT1305	Q8KCV5	Outer Membrane	Uncharacterized protein
CT1353	Q8KCR0	Outer Membrane	OmpA family protein
CT1447	Q8KCH4	Periplasmic	Serine protease (manually annotated as DegP)
CT1804	Q8KBI3	Outer Membrane	Uncharacterized protein
CT1943	Q46367	Unknown	Chlorosome protein C
CT1953	Q8KB41	Outer Membrane	TonB receptor family
CT2049	Q8KAV2	Outer Membrane	LipD protein, putative
CT2144	Q8KAL2	Outer Membrane	Outer surface protein, putative
CT2264	Q8KAA2	Periplasmic	Peptidyl-prolyl cis-trans isomerase SurA

870

871 **Table 1.** The OMV core proteome consists of 28 proteins found in OMVs, S(0) globules and
872 whole cells.